Studies in Health Technology and Informatics

This book series was started in 1990 to promote research conducted under the auspices of the EC programmes' Advanced Informatics in Medicine (AIM) and Biomedical and Health Research (BHR) bioengineering branch. A driving aspect of international health informatics is that telecommunication technology, rehabilitative technology, intelligent home technology and many other components are moving together and form one integrated world of information and communication media. The complete series has been accepted in Medline. Volumes from 2005 onwards are available online.

Volume 132

Recently published in this series

Vol. 131. R. Latifi (Ed.), Current Principles and Practices of Telemedicine and e-Health
Vol. 130. J.I. Westbrook, E.W. Coiera, J.L. Callen and J. Aarts (Eds.), Information Technology in Health Care 2007 – Proceedings of the 3rd International Conference on Information Technology in Health Care: Socio-technical Approaches
Vol. 129. K.A. Kuhn, J.R. Warren and T.-Y. Leong (Eds.), MEDINFO 2007 – Proceedings of the 12th World Congress on Health (Medical) Informatics – Building Sustainable Health Systems
Vol. 128. P.J. Murray, H.-A. Park, W.S. Erdley and J. Kim (Eds.), Nursing Informatics 2020: Towards Defining Our Own Future – Proceedings of NI2006 Post Congress Conference
Vol. 127. L. Bos and B. Blobel (Eds.), Medical and Care Compunetics 4
Vol. 126. N. Jacq, H. Müller, I. Blanquer, Y. Legré, V. Breton, D. Hausser, V. Hernández, T. Solomonides and M. Hofmann-Apitius (Eds.), From Genes to Personalized HealthCare: Grid Solutions for the Life Sciences – Proceedings of HealthGrid 2007
Vol. 125. J.D. Westwood, R.S. Haluck, H.M. Hoffman, G.T. Mogel, R. Phillips, R.A. Robb and K.G. Vosburgh (Eds.), Medicine Meets Virtual Reality 15 – *in vivo, in vitro, in silico*: Designing the Next in Medicine

ISSN 0926-9630

Medicine Meets Virtual Reality 16

parallel, combinatorial, convergent: NextMed by Design

Edited by
James D. Westwood
Randy S. Haluck MD FACS
Helene M. Hoffman PhD
Greg T. Mogel MD
Roger Phillips PhD CEng FBCS CIPT
Richard A. Robb PhD
and
Kirby G. Vosburgh PhD

IOS Press
Amsterdam • Berlin • Oxford • Tokyo • Washington, DC

Medicine Meets Virtual Reality 16
J.D. Westwood et al. (Eds.)
IOS Press, 2008

Collaborative Engineering: 3-D Optical Imaging and Gas Exchange Simulation of *In-Vitro* Alveolar Constructs

Jannick P. ROLLAND[1,3], Kye-sung LEE[1], Ayesha MAHMOOD[7], Lisa FLUCK[1,2], Jaime DUARTE[2], Ilhan KAYA[3], Anand SANTHANAM[1,6], Panomsak MEEMON[1], Supraja MURALI[1], Olusegun ILEGBUSI[2], Patrick KUPELIAN[6], William L. WARREN[7], Peter MOLNAR[4], James HICKMAN[4], and Papachan KOLATTUKUDY[5]
[1]*CREOL, College of Optics and Photonics,* [2]*Mechanical Materials and Aerospace Engineering,* [3]*School of Electrical Engineering and Computer Science,* [4]*NanoScience Technology Center,* [5]*Burnett School of Biomedical Sciences in The College of Medicine University of Central Florida, Orlando, Florida 32816*
[6]*M.D. Anderson Cancer Center Orlando, Orlando, Florida 32806*
[7]*VaxDesign Corporation, Orlando, Florida 32826*

Abstract. This paper reports on the computational simulation and modeling of an *in vitro* alveolar construct system along the optical coherence microscopy (OCM) methods for visualizing engineered tissue. The optical imaging methods will be compared to immunohistochemical light microscopy samples of engineered alveolar constructs. Results show depth images of the alveolar tissue construct for a bilayer construct, as well as predictions of the gas exchange process in a simple model of a bio-reactor hosting the construct.

Keywords. Tissue engineering, Alveolar tissue constructs, Optical coherence microscopy, Optical coherence tomography, Gas exchange simulation.

1. Introduction

Tissue engineering is driven in large part by the potential for creating functional tissues and organs for much-needed transplants. Also, tissue engineering of immunological constructs can provide alternatives, if composed of biologically relevant primary cell types, to animal studies in the development of preventive or healing drugs. Such tissue engineered systems provide ideal means of studying localized tissue responses to pathogens and therapeutic treatments in an accurate and cost effective manner.

We describe a research effort that focuses on developing methods for engineering *in-vitro* alveolar tissue constructs. We hypothesize that in order to dissect the mechanisms of immunity, bio-imaging and computational science are necessary to visualize, monitor, model and characterize adequately the architecture of the engineered tissue. The reported gas exchange modeling and simulation studies are also providing insight into the design of the bioreactor housing the alveolar constructs.

2. Background

2.1. Tissue Imaging

Visualization of in-vitro grown tissue via various microscopic methods provide means of overall tissue characterization from macroscopic structural resolution and down to cellular level along with functional protein or disease specific marker identification. Historically, non-invasive imaging methods, like light microscopy (LM), have resolution limitations in imaging opaque or dense tissue and therefore more advanced laser microcopy methods such as confocal imaging, optical coherence imaging, and radiology are gaining much interest to visualize tissue structure by non-destructive means. Here, we report the usefulness of Optical Coherence Microscopy (OCM) to identify the tissue architecture of in-vitro cultured alveolar constructs, where immunohistochemical analysis, will be used as a comparative measure of optical resolution between OCM and histology [1].[1].

OCM is a noninvasive high resolution and high sensitivity depth-resolved imaging technique [2]. OCM performs cross-sectional tomographic imaging of the internal microstructure in materials and biological systems by measuring backscattered or backreflected light. Axial resolution is determined by the coherence length of the source. The transverse resolution depends on the numerical aperture of the objective lens. With OCM, it is possible to image cellular structures at certain depth below the tissue surface. Resolutions as small as the microns can be achieved with OCM, while in practice, high resolution OCM reports around 2.5-3.5 μm on both axial and lateral resolutions [2]. Recently OCM was used as an imaging modality to monitor non-invasively the engineered tissue models composed of chitosan scaffolds with fibroblasts [3] and porous scaffolds with bone cells [4].

2.2 Gas exchange process

The gas exchange process at the alveolar level occurs by simple diffusion of molecules from regions of high to low concentration [5,6]. Air arrives at the respiratory zone with an oxygen (O_2) partial pressure (concentration) of 100 mmHg and a carbon dioxide (CO_2) concentration of 40 mmHg. The CO_2 concentration results from steady replenishment of the CO_2 ventilated out of the lungs, assuming sufficient inside-out diffusion from the blood, where the combined concentration of the CO3(--), HCO3(-) and CO2 forms, in which CO2 is carried in blood, is very high. On the other hand, the blood in the pulmonary capillary is depleted of oxygen and is rich in CO_2 with concentration values of 40 mmHg and 46 mm, respectively. Fick's law of diffusion dictates that the amount of gas that diffuses across a sheet of tissue is proportional to it's the surface area of the sheet but inversely proportional to its thickness. Based on these partial pressure gradients, O_2 diffuses from the alveoli into the blood, while CO_2

[1] The alveolar mucosal constructs and the reference LM immunohistochemical work was conducted at VaxDesign Corporation.

diffuses from the blood into the alveoli. In a real respiratory system, the conducting airways represent a much larger reservoir of air relative to the blood in the pulmonary capillary, such that the partial pressures of O_2 and CO_2 remain essentially constant with time. The diffusion process thus reaches equilibrium when the O_2 and CO_2 concentration levels in the pulmonary capillary are 100 mmHg and 40 mmHg, respectively. Although blood spends approximately 0.75 second in the pulmonary capillaries, the complete exchange process takes only about 0.25 s [5].

2.3 Estimation of regional alveolar ventilation (RAV)

Regional alveolar ventilation (RAV) is a key biological parameter that illustrates the amount of air entering the alveoli for every breathing cycle. RAV forms a key input for the gas exchange simulation since RAV varies inside human lungs. RAV varies from subject to subject based on the physiological condition of the subject (normal or a diseased state). Conventional methods of estimating RAV using plethysmograpy do not account for regional variations [5]. Image-based methods use inhaled or injected tracers for estimating RAV [7]. Such methods are limited by the resolution of the captured image and the error induced by the non-gated nature of imaging as well as the voluntary and involuntary changes in the breathing pattern. Biomathematical models [8] coupled with 4D Computed Tomography are investigated to estimate RAV at a higher resolution and accuracy compared to image-based methods with tracers.

3. Methods

3.1 Tissue engineered alveolar construct fabrication and histology

Tissue fabrication and immunohistochemical staining protocols were similar to an earlier report [1]. Briefly, the alveolar mucosal constructs were prepared by creating a bilayer cellular structure on top of a collagen and laminin coated Transwell membranes of known 10μm thickness and pore density of $4x10^6cm^2$. Alveolar endothelial cells were cultured until confluency. Alveolar epithelial cells were then seeded on top of the endothelium to create an epithelium. Cells were purchased from ScieneCell (passage 4-8). Control samples included dry coated and media hydrated membranes, along with endothelium, and epithelium containing constructs. Standard culture conditions were applied (37°C, 5% CO_2). Epithelial cells in the bilayer construct were identified by immunohistochemical staining of alveolar cell specific cytokeratins including CK-1, 4, 5, 6, 8, 10, 13, 18, 19. The endothelial cells were identified by Factor VIII staining. Formalin fixed tissue samples were paraffin embedded and sectioned into 5μm slices prior to antibody staining. The tissue was then deparaffinized and serum blocked. Each primary antibody was applied followed by biotinylated secondary antibody incubation. Strepavidin-peroxidase enzyme conjugate was then applied and aminoethyl carbazole (AEC) chromogen was used for color development. Light microscopy was performed using a Olympus Fluoview Confocal Microscope (FV10-SW). Primary and secondary antibodies were purchased from Invitrogen. Engineered tissue construct samples for light microscopy were fixed in formalin and stored at 4°C prior to embedding and immunohistochemical analysis. Samples for OCM were kept in culture media before and during imaging at room temperature (~27°C).

3.2 Optical coherence microscopy imaging apparatus

The OCM system consisted of a Titanium:sapphire laser (Femtosource Integral OCT; Femtolasers Inc.) with a spectral bandwidth of 120 nm centered at 820 nm corresponding to ~2.5 μm axial resolution in air. The detection system was a spectrometer with a 3648 CCD pixel line array (HR 4000; Ocean optics Inc.). In this imaging system, 80% of the beam intensity from the coupler was collimated with a 2 mm diameter beam size (full width at $1/e^2$) and then incident on a 20X magnification, 0.12 NA microscope objective integrated into the sample arm of the OCM system. The light was then focused on the sample, achieving about 4 μm in transverse resolution with a depth of field of approximately 100 μm in air. The system sensitivity was 97dB. The remaining 20% of beam intensity was reflected by a mirror through a Fourier domain optical delay line located in the reference arm, whose main function was to control the overall dispersion in the system. Polarization was also adjusted to yield maximal signal modulation depth. The 3D dataset of 200 x-z images with 200 axial scans was collected for each sample set in about 70min. The x-y en face OCM images were then reconstructed with 200 μm by 200 μm field of view.

3.3 Simulation of the gas exchange process

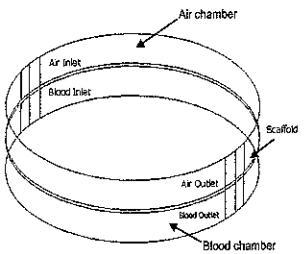

Figure 1. Schematic representation of the bioreactor

In order to model the gas exchange process, a 3D virtual construct illustrated in Fig. 1was created to represent the three volumes participating in the diffusion process: a gas chamber representing the respiratory airways; a scaffold representing the alveolar membrane (surfactant, epithelium, and endothelium); and a test fluid chamber which represents the pulmonary capillary containing the oxygen containing media, i.e., blood. Although the model has been created to initially simulate diffusion under stagnant conditions, it can readily be modified to accommodate air and fluid flow. In the next steps (not reported herein), we will place the engineered alveolar tissue in the bioreactor. The modeling aspects are assisting in our experimental studies to ascertain geometries and configurations for realistic gas exchange conditions.

Both blood and air are assumed to be stagnant, and initially have uniform concentrations of O_2 and CO_2 corresponding to the physiological partial pressures. The input parameters are provided in [5]. The physical process involved is the diffusion of O_2 and CO_2. The boundary conditions have been set at fixed concentration values of 40 mmHg for CO_2 and 100 mmHg for O_2 in the air chamber: These conditions simulate the constant renewal of alveolar air that results in constant concentration of O_2 in the alveoli during respiration and adequate CO_2 replenishment due to inside-out diffusion from capillary to the alveoli. Strictly, the CO_2 boundary condition should be obtained from experiments. The condition imposed here was considered reasonable for the stagnant situation simulated and could be readily relaxed for a subsequent non-stagnant analysis. In the scaffold and the blood chamber, we set a fixed flux of zero at the walls for O_2 and CO_2. At the air-scaffold and scaffold-blood interfaces, the diffusive flux normal to the boundary is conserved. Separate diffusion equations are then solved for

O_2 and CO_2 in both blood and air chambers, subject to the above boundary conditions. It should be noted that this approach inherently accounts for both the inside-out diffusion of CO_2 and the outside-in diffusion of O_2 across the membranes.

3.4 Extraction of RAV for the simulation of non-stagnant gas exchange analysis

A mathematical inverse using Spherical Harmonics (SH) [9] and a physical inverse method [10] to estimate the elasticity of a 3D lung surface model from its change in shape have been previously investigated. Specifically, the SH representation was used in conjunction with the 3D lung surface model for establishing the 3D tissue elasticity. We extend the mathematical inverse method for estimating the RAV using a Hyper Spherical Harmonic (HSH) transformation [11] representation in conjunction with 4D Computed Tomography images. HSH transformations can represent the force applied and the local elastic interactions of a 3D lung volumetric model as a set of hyper-spherical functions. They involve an extension of SH transformations.

4 Results and Discussion

4.1 High resolution optical coherence imaging of engineered lung tissue

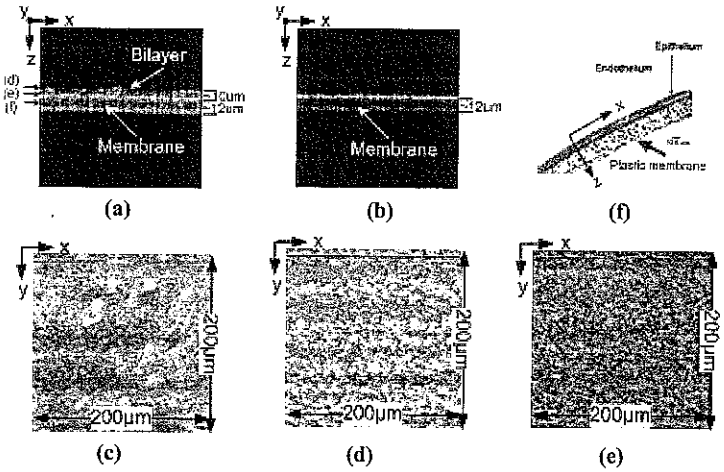

Figure 2. Optical coherence (OCM) and light microscopy (LM) images of the bilayer alveolar tissue constructs.
OCM*: (a) A cross section OCM image where arrow "d" points to the epithelium, "e" endothelium and "f" membrane structures **(b)** A cross section OCM image of a membrane only, and top view (en face) images of an **(c)** epithelium layer, **(d)** endothelium layer and **(e)** inside a membrane. The top view image size is 200µm by 200µm.
LM: f)** 5µm cross-sectional histology image of the bilayer construct showing an epithelium and an endothelium along with the porous membrane.
* scale bars for the OCM images are based on estimated material and media refractive indices;
** reference image provided by VaxDesign Corporation.

Figure 2 shows the images of a bilayer cell sample that is composed of one epithelium and one endothelium layers and a membrane. Fig.2(a) is a cross section (x-z) image of the sample by OCM and Fig.2(b) is a cross-section image of the membrane alone. The thickness of the epithelium, the endothelium and the membrane were measured to be approx. 6µm, 4µm, and 12µm, respectively. The thicknesses were calculated based on the media index 1.33 for the tissue and the refractive index of polyester 1.6 for the membrane. The engineered lung tissue on the membrane in Fig.2(a) was identified when compared with the membrane only image in Fig.2(c). The top view (en face) images of the epithelium and endothelium layers and the membrane were taken at about 4 µm below the surface in Fig.2(d), 8 µm below the surface in Fig.2(e), and 16 µm below the surface in Fig.2(d), and Fig.2(e) shows a top view layer image in the middle of the membrane. Fig.2(f) shows a light microscopy reference image of the bilayer construct with distinctive epithelium and endothelium layers on top of a porous membrane.

4.2 Simulation of the gas exchange

This study focused on the effect that the surface-to-volume ratio (S/V), a geometric property, would have on the time required for the tissue engineered system described above to reach equilibrium. The S/V in the present situation describes the ratio of the alveolar surface area to the volume of air chamber. As mentioned earlier, the concentrations of O_2 and CO_2 were set to remain constant in the air chamber. For the first study, a simple geometry was modelled and the total height of the system was changed while maintaining the same diameter in order to affect the S/V ratio. Modifying the total height of the system would ultimately affect the volume thereby affecting the S/V. Figure 3a presents the predicted threshold time as a function of the S/V ratio. The result indicates that the threshold time to reach physiological concentration decreases exponentially as the S/V ratio increases. This result is plausible as the higher S/V ratio presents very large surface area for diffusion to occur rapidly across the membrane. The S/V ratio is clearly an important factor that needs to be taken into account when designing and modelling surrogate gas-exchange processes as it significantly affects the time for the system to reach equilibrium.

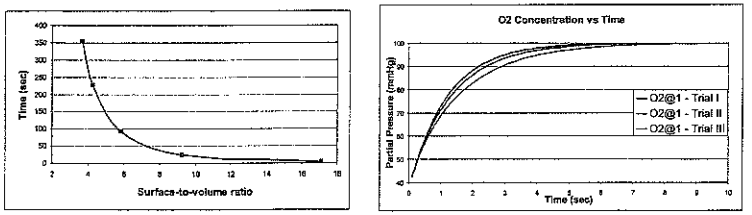

Figure 3. (a) Predicted time needed to reach O_2 physiological values vs. the surface-to-volume ratio. **(b)** Predicted O_2 concentration for varying height of air chamber.

The effect of varying air-chamber height on the O_2 concentration in the blood is presented in Fig.3b. The objective is to assess the influence of the boundary conditions

imposed on the gaseous components in the air chamber. The diameter is kept constant while three air chamber heights of 5.10^{-5}m (top), 1.10^{-4}m (middle) and 2.10^{-4}m (lower) are considered. The figure indicates there is no significant difference in the time required to reach equilibrium between the three cases, thereby justifying the boundary condition used to represent infinite gas supply in the air chamber.

5 Conclusion

In vitro tissue engineering research relies on multi-disciplinary expertise and promises alternatives to animal models in the development of preventive or healing drugs. In this work we described a collaborative project in tissue engineering where modeling, simulation, and imaging play an essential role in the design of the bioreactor and that of the alveolar engineered tissue constructs. Such collaborative effort aims to bring forth subject-specific human surrogates to therapy and immunology studies to tailor treatments to individual human conditions.

Acknowledgements

This work is supported by the US Army Medical Research and Material Command, M.D. Anderson Cancer Center Orlando, the UCF I^{2}Lab Foundation, and DARPA/DSO.

Reference

[1] A. Mahmood, A. Kachurin, E. Mishkin, and W. Warren. *Design and evaluation of engineered alveolar mucosal constructs for respirology* Annual Society of Biomedical Engineers, Los Angeles, CA, 2007.

[2] B.E. Bouma and G.J. Tearney, *Handbook of Optical Coherence Tomography*, New York, Marcel Dekker, 2002.

[3] W. Tan, A.S. Urkmez, L.J. Fahrner, R. Jamison, D. Leckband, and S.A. Boppart. "Structural and functional optical imaging of three-dimensional engineered tissue development," *Tissue Eng.* **10**, 1747–1756, 2004.

[4] Y. Yang, A. Dubois, X. Qin, J. Li, A.E. Haj, and R.K. Wang, "Investigation of optical coherence tomography as an imaging modality in tissue engineering," *Phys. Med. Biol.* **51**, 1649-1659, 2006.

[5] J.B. West, *Respiratory physiology, the essentials*. Philadelphia,USA: Lippincott Williams and Wilkins. 1995.

[6] E. Mates van Lõbensels, J.C. Anderson, J. Hildebrandt, and M.P. Hlastala. *Modeling diffusion limitation of gas exchange in lungs containing perfluorocarbon.* J. Appl. Physiol. **86,** 273-284, 1999.

[7] J. Richard, M. Janier., F. Lavenne, C. Tourvieille, D. Bars, N. Costes, G. Gimenez, C. Guerin, *Quantitative assessment of regional alveolar ventilation and gas volume using N-N2 washout and PET.* Journal of Nuclear Medicine **46** (8), 1375-1383, 2005.

[8] A. Santhanam et al., *Modeling and simulation of Real-time 3D lung dynamics.* IEEE Transactions on Information Technology and Biomedicine, 2007.

[9] A. Santhanam, A. and J.P. Rolland. *An Inverse deformation method for the visualization of lung dynamics*. In *Fourth Intern. conference on Ultras. imaging and tissue elasticity.* Austin TX. 2005.

[10] A. Santhanam, and J.P. Rolland. *An inverse 3D lung deformation analysis for medical visualization. In Computer Animation and Social Agents.* Geneva, Switzerland: Computer Graphics Society, 2006.

[11] J. Avery, *Hyperspherical harmonics and generalized sturmains.* Progress in theoretical chemistry and physics. Boston, MA: Kluwer Academic Publishers, 2000.

Medicine Meets Virtual Reality 16
J.D. Westwood et al. (Eds.)
IOS Press, 2008

A Virtual Reality Throat Examination Simulation

G S RUTHENBECK [a], H OWEN [b], K J REYNOLDS [a]
[a] *School of Informatics & Engineering, Flinders University, South Australia*
[b] *School of Medicine, Flinders University, South Australia*

Abstract. Computer based patient simulators can provide an alternative to inanimate clinical skills training. Here we present a virtual reality throat examination simulation capable of simulating a range of throat pathologies. The computer interface employs haptic feedback to allow students to interact naturally with the software.

Keywords. Virtual Reality, VR, Part Task, Medical Simulation, Haptic Interface, Throat Examination Simulator, clinical skills training.

Introduction

Clinical skills education is enhanced by deconstructing the skills and teaching them in parts [1,2]. Patient simulators are useful learning aids and part task trainers are widely used for teaching a range of procedures [3,4]. Some skills are greatly affected by patient cooperation and some need to be completed in a short time. Competence in these skills cannot be learnt or tested on inanimate models, and it is not appropriate or feasible to use actual or standardised patients for this. It is a challenge for medical schools to provide students with the skills training and assessment necessary for them to become safe and effective medical practitioners.

Competence in a clinical skill requires deliberate practise in context with specific feedback [5,6]. Computer screen-based simulators have been used to support acquisition of knowledge associated with clinical skills (eg Microsim™, Laerdal) and more recently haptic devices have been used for learning invasive clinical skills (e.g. cricothyrotomy). We have developed a simulator that incorporates knowledge and skill learning elements for a core diagnostic clinical skill in a flexible platform that can be applied to many other skills.

1. Tools/Methods

The simulator has been developed for desktop computers (running Windows, MacOS, or Linux). It allows students to practice performing oral examinations. A Sensable Phantom Omni has been used as the input device because the user's manipulations of the stylus translate directly to movements of tools within the virtual scene. In so doing, users practice movements similar to when performing the procedure on real patients.

Haptic feedback is provided for interactions between key structures to enhance immersion and consequently facilitate learning. Stereoscopic 3D display is supported (via flicker glasses etc) to provide depth information required for intuitive interaction.

The simulation presents the user with the head and shoulders of a patient (Figure 1). The virtual patient must be requested to open their mouth (via a button press) at